Dalton Transactions

ROYAL SOCIETY OF CHEMISTRY

PAPER

View Article Online
View Journal | View Issue

Cite this: *Dalton Trans.*, 2025, **54**, 12678

Structure, magnetism and thermal stability of the n = 3 Ruddlesden–Popper oxyfluoride $La_4Ni_3O_{8.4}F_{3.5}$†

Jakob Geßner, Stefan G. Ebbinghaus and Jonas Jacobs *

Oxides of the Ruddlesden–Popper (RP) series $A_{n+1}B_nO_{3n+1}$ are ideal candidates for the incorporation of additional anions like F^-, H^-, or N^{3-} in the crystal lattice. The resulting mixed anionic compounds usually exhibit clearly different physical properties compared to the precursor oxides due to changes in their atomic and electronic structures. We present the synthesis of the highly fluorinated n = 3 oxyfluoride $La_4Ni_3O_{8.4}F_{3.5}$ by topochemical fluorination of $La_4Ni_3O_{10}$, with poly(vinylidene difluoride) (PVDF) as the fluoride source. The structure of this compound was solved based on X-ray and neutron powder diffraction data. A monoclinic ($P2_1/a$, a = 5.4206(3) Å, b = 5.5081(3) Å, c = 29.9823(18) Å, and β = 90.85(4)°) distorted variant of the n = 3 RP structure was found showing a strong elongation perpendicular to the perovskite slabs resulting from full occupation of the interstitial anion positions. The formation reaction and the decomposition reaction were investigated by *in situ* X-ray diffraction. By this, the presence of one distinct formation intermediate was revealed. The thermal decomposition was found to start at 490 °C, accompanied by the release of oxygen as detected by coupled mass spectrometry. Temperature and field dependent magnetization measurements indicate that the title oxyfluoride is a Curie–Weiss paramagnet, in contrast to the parent oxide, which shows Pauli paramagnetism, highlighting the strong impact of anion substitution on the physical properties of these mixed anionic compounds.

Received 14th May 2025,
Accepted 20th July 2025

DOI: 10.1039/d5dt01138h

rsc.li/dalton

Introduction

The crystal structure of Ruddlesden–Popper (RP) oxides can be described as alternating stacks of n perovskite layers ABO_3 and one single rock salt layer AO. This stacking results in the general formula $A_{n+1}B_nO_{3n+1}$, where n = 1, 2, 3 or even higher.[1,2] Here, A is often a lanthanide or alkaline earth ion and B in most cases is a transition metal cation.[3]

Mixed anion Ruddlesden–Popper oxides often exhibit interesting physical properties such as band gap values in the range of the solar spectrum,[4,5] ferroelectricity,[5–7] ionic transport,[8,9] or altermagnetism.[10,11] There are even examples showing high-temperature superconductivity.[12,13]

In the highest symmetric version of the n = 3 RP structure (space group: $I4/mmm$ (Fig. 1)), four different anionic sites exist, which form the vertices of the BO_6 octahedra of the perovskite slab: central apical (*ca*, 4*e*, (0,0,z_1)), central equatorial (*ce*, 4*c*, ($\frac{1}{2}$,0,0)), terminal apical (*ta*, 4*e*, (0,0,z_2)) and terminal equatorial (*te*, 8*g*, ($\frac{1}{2}$,0,z_3)). In addition, a fifth anion site is located within the rock salt layer (*i*, 8*f*, ($\frac{1}{4}$,$\frac{1}{4}$,$\frac{1}{4}$)), which is usually unoccupied but can take up to two additional anions per formula unit.

Other ions, such as nitride,[4,5] hydride,[14,15] hydroxide,[16,17] halide[3,8,18–21] or even carbonate[22] ions, can be located on these interstitial sites, resulting in mixed anionic materials with different properties compared to the corresponding oxides. This additive insertion of anions in the rock salt-type layer often results in an increase of the average oxidation number of the cations. The formation of such mixed anionic compounds can also occur from partial substitution of O^{2-} ions, where in the case of O^{2-}/F^-, a substitution on the apical sites is often found to be favored over a statistical distribution to the apical and equatorial sites.[23]

For the more comprehensively investigated group of n = 1 RP oxyfluorides, there are examples of both anion substitution scenarios: in K_2NbO_3F, the fluoride ions occupy the apical vertices in a disordered manner,[24,25] whereas in Sr_2FeO_3F, the apical sites are occupied in an ordered way. Due to the increased Fe–F bond length compared to the Fe–O bond length, this substitution leads to square-pyramidal coordination of the Fe^{3+} ions.[21,26] Examples for the insertion of F^- into the interstitial sites are $La_2CoO_4F_{1.2}$ with unordered occupation,[27] $LaSrMnO_4F$ with layer-wise ordering of fluoride-occupied and empty interstitial sites[28] and $Ba_{2-x}Sr_xPdO_2F_2$, where the interstitial sites are fully occupied, resulting in a square-

Martin Luther University Halle-Wittenberg, Faculty of Natural Sciences II, Institute of Chemistry, Inorganic Chemistry, Kurt-Mothes-Straße 2, 06120 Halle, Germany.
E-mail: jonas.jacobs@chemie.uni-halle.de

† Electronic supplementary information (ESI) available. See DOI: https://doi.org/10.1039/d5dt01138h

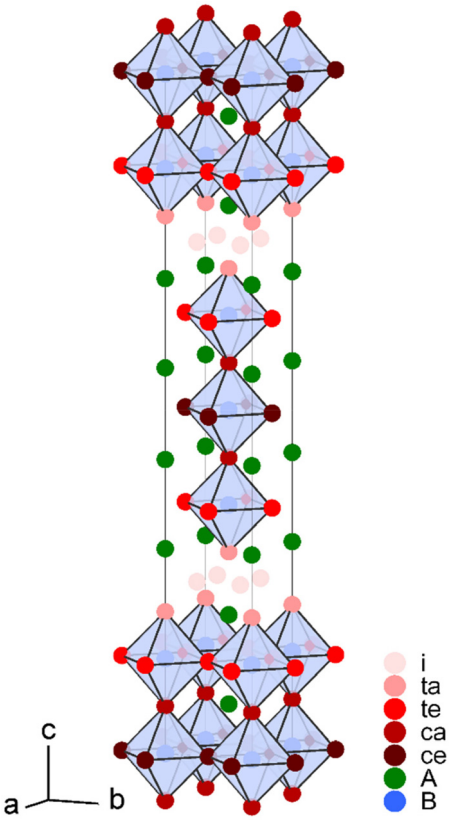

Fig. 1 Representation of the ideal n = 3 Ruddlesden–Popper structure (space group: *I*4/*mmm*). The BO_6 octahedra are shown and the different anion sites are indicated by different shades of red.

planar coordination of Pd^{2+}.[29] Finally, there are compounds where both anion sites, apical and interstitial, are occupied by fluoride, *e.g.*, $La_2NiO_{2.5}F_3$[19] or $Sr_2TiO_3F_2$.[30] To our knowledge, there are no n = 1 RP oxyfluorides, where the equatorial sites are solely occupied by F^-.

For the n = 2 RP oxyfluorides, there are also reports on a variety of anion ordering scenarios with examples of F^- occupying only interstitial sites,[31,32] only terminal apical sites,[33,34] or both interstitial and terminal apical sites as in $La_3Ni_2O_{5.5}F_{3.5}$[35] or other related compounds.[36,37] As with the n = 1 case, there are no studies indicating occupancy of the equatorial vertices of the octahedra by F^-. Furthermore, to the best of our knowledge, no fluoride occupation of central apical anion sites has been reported, either.

Only very few n = 3 RP oxyfluorides are known so far. The four compounds $La_{0.5}Sr_{3.5}Fe_3O_{7.5}F_{2.6}$,[3] $La_4Co_3O_{10}F_2$,[38] $La_4Ni_3O_8F_{0.84}$,[39] and $La_4Ni_3O_8F_{1.7}$[39] are the only members described in the literature to date. For all compounds, an increase in the unit cell parameter c was found, compared to that of the parent oxides. With a Δc of ~3 Å, a clear sign of a full interlayer occupation was found for $La_4Co_3O_{10}F_2$, while for $La_{0.5}Sr_{3.5}Fe_3O_{7.5}F_2$ with a Δc of ~1.2 Å, only a partial interlayer occupation in combination with a fully terminal apical occupation was derived from refinement of neutron powder diffraction data. The nickel compounds $La_4Ni_3O_8F_{0.84}$ and $La_4Ni_3O_8F_{1.7}$ were obtained from fluorination of the reduced RP-oxide $La_4Ni_3O_8$ with XeF_2. A partial O/F ordering and the presence of highly elongated NiO_4F_2 octahedra were derived based on X-ray diffraction data. The elongated octahedra were seen as an indication of the occupation of the terminal apical anion sites by F^-.

Different methods are applied to obtain such oxyfluorides. The fluorination applied here follows the low-temperature route first described by Slater.[40] The use of fluorinated organic polymers such as poly(vinylidene difluoride) (PVDF; $(CH_2F_2)_n$) often yields oxyfluorides of higher quality than other fluorinating agents such as NH_4F, CuF_2, or F_2-gas, which are sometimes difficult to handle and whose products tend to remain as impurities in the obtained samples.[41–45] The PVDF-based fluorination method was also applied to obtain the above-mentioned n = 3 compounds, $La_{0.5}Sr_{3.5}Fe_3O_{7.5}F_{2.6}$[3] and $La_4Co_3O_{10}F_2$,[38] as well as the n = 1 nickelate oxyfluorides, $La_2NiO_3F_2$[46,47] and $La_2NiO_{2.5}F_3$.[19]

In this study, we present the successful synthesis of the n = 3 RP oxyfluoride with the formula $La_4Ni_3O_{8.4}F_{3.5}$, which was synthesized by topochemical fluorination of $La_4Ni_3O_{10}$, obtained from citrate synthesis, with PVDF as the fluorine source. The oxyfluoride crystallizes in the monoclinic space group $P2_1/a$. Its structure was solved by Rietveld refinement based on neutron and X-ray powder diffraction (XRD) data in combination with elemental analysis methods (*e.g.* XRF, iodometric titration, and F^- determination by ISE). *In situ* XRD experiments were used to trace the formation reaction and the thermal decomposition reaction of the oxyfluoride. Here, the presence of reaction intermediates, one for the formation and two for the decomposition, each with different crystal structures, was revealed. The observation of the decomposition intermediates is accompanied by the release of oxygen as identified *via* mass spectrometry. The temperature- and field-dependent magnetic behavior was also investigated and a change from the Pauli paramagnetism of the precursor oxide to Curie–Weiss paramagnetism is found for $La_4Ni_3O_{8.4}F_{3.5}$.

Experimental section

Synthesis

The synthesis of $La_4Ni_3O_{8.4}F_{3.5}$ was performed by a two-step procedure. First, the precursor oxide $La_4Ni_3O_{10}$ was synthesized by a citric acid complexation method. Stoichiometric amounts of La_2O_3 (Chempur, 99.99%; dried at 900 °C for 3 h) and Ni powder (VEB-Jenapharm, 99.5%) were dissolved in demineralized water by dropwise addition of concentrated HNO_3. Citric acid (Grüssing) was added in a molar ratio of 3 : 1 to the metal cations under stirring. Water was evaporated from the solution on a hot plate until a gel-like substance was obtained. Further heating of this gel at 350 °C resulted in self ignition. The resulting material was further heated in a box furnace at 450 °C for 6 h to decompose the remaining organic compounds. The resulting blackish powder was then ground in an agate mortar and calcined at 1000 °C for 24 h.

Fluorination was performed by mixing the precursor oxide with PVDF (Alfa Aesar) in a 1 : 2 ratio according to the mass of its monomeric unit CH_2CF_2. The mixture was heated in air at 370 °C for 16 h and allowed to cool down to room temperature, yielding the final oxyfluoride.

Characterization

Room temperature powder X-ray diffraction (XRD) patterns were recorded in the angular range of 2θ = 10–140° with a step size of 0.01° and a time of 3 s per step with Cu-$K_{\alpha1,2}$ radiation on a Bragg–Brentano Bruker AXS D8 Advance diffractometer equipped with a LYNXEYE silicon strip detector. In addition, a STOE STADI MP diffractometer with transmission geometry and monochromatic Mo-$K_{\alpha1}$ radiation equipped with a DECTRIS MYTHEN 1 K detector was also used for room temperature scans in the angular range of 2θ = 5–85°.

The latter diffractometer was also used to collect variable temperature XRD data with a STOE capillary furnace. These patterns were recorded in the angular range of 2θ = 8–44°. To follow the formation reaction of the oxyfluoride, the sample was heated up to 370 °C and diffraction patterns were recorded every 7 minutes. To study the decomposition processes of the oxyfluoride in oxidative and reductive atmospheres (N_2, air, and O_2), heating was performed from 50 °C to 250 °C in steps of 50 K at 50 K min^{-1}, then in steps of 10 K at 10 K min^{-1} in the range of 250–650 °C and ith Cin steps of 25 K at 25 K min^{-1} from 650–900 °C. After each heating step, a XRD scan with an acquisition time of ∼10 min was performed. The transfer capillary of a mass spectrometer (Pfeiffer Vacuum OmniStar GSD 350) was inserted in the sample capillary using a self-made setup (compare Fig. S1†) allowing for the simultaneous analysis of the gaseous reaction products.

Neutron diffraction (ND) data of $La_4Ni_3O_{8.4}F_{3.5}$ were collected on the high-resolution powder diffractometer D2B at the Institute Laue-Langevin in Grenoble, France. Beamtime was granted under Proposal 5-23-769 [48] and measurements of the 1.1 g sample (in a 6 mm V-cylinder) was performed at 300 K with λ = 1.594 Å and an acquisition time of about 3 h.

Joint Rietveld refinements of XRD and ND data were performed using the GSAS-II software.[49] Instrumental resolution parameters for the Bruker D8-Advance diffractometer were determined from the refinement of an α-Al_2O_3 reference scan. LaB_6 was used as the reference material to determine the instrumental resolution parameters for the STOE STADI MP diffractometer.

Magnetic measurements were carried out using the ACMS option of a Quantum Design PPMS-9. Approximately 100 mg of the powder samples (oxide and oxyfluoride) were loaded in gelatin capsules, which were then attached to the end of a plastic straw. The gelatin capsules ensure a low diamagnetic contribution to the measured susceptibilities. The temperature dependent moment was measured at an external field of 0.1 T and 5 T in the temperature range of 5–300 K. For B = 0.1 T zero-field-cooled (ZFC) and field-cooled (FC) conditions were applied. The data for the measurement in B = 5 T was collected while warming the previously field-cooled sample (FCW). The field dependence of the magnetic behavior was analyzed by recording the complete hysteresis from −5 to 5 T at 5 K.

The oxygen content of both the oxide and the oxyfluoride was determined by thermogravimetric analysis (TGA) using a TA Instruments TGA550 thermobalance under flowing forming gas (furnace gas: 10% H_2 in N_2, 25 mL min^{-1}; balance protecting gas: N_2, 25 mL min^{-1}). The samples were heated to 950 °C at 10 K min^{-1} and held at this temperature for 10 min to ensure a full reduction.

The fluorination product was checked for residual PVDF as well as other carbon related impurities by infrared (IR) spectroscopy (Bruker Alpha) in the $\tilde{\nu}$ range of 4000–400 cm^{-1}.

The contents of La and Ni were quantified by X-ray fluorescence spectroscopy (XRF) (Panalytical Epsilon 4) using the standardless quantification mode (Omnian mode).

The average oxidation states of Ni in the precursor oxide and the oxyfluoride were determined by iodometric titration. Approximately 15 mg of the samples were dissolved in 5 M HCl containing an excess of KI. Afterwards, ∼1 g of Na_2CO_3 was added to provide a pseudo inert atmosphere of CO_2. A 0.006 M $Na_2S_2O_3$ solution was used as the titrant with starch solution as the indicator. The oxidation state was averaged from three independent measurements per sample.

The amount of fluoride was quantified using a Mettler Toledo SevenMulti ion sensitive electrode (ISE). In a 100 mL PMP volumetric flask, ∼10 mg of the sample was dissolved in 10 mL of 5 M HCl. The dissolved cations were complexed with 10 mL of a Titriplex IV solution (c = 6.82 g L^{-1}). The pH value was adjusted to ∼6 against the bromothymol blue indicator by adding a CH_3COOH/CH_3COONa buffer and NaOH solution (c = 5 mol L^{-1}). The flask was then topped with demineralized water. The F^- content was obtained from standard addition (40 mL sample solution, addition of 5 × 100 µL of a 1 g L^{-1} F^- standard solution (Mettler Toledo) using a single channel pipette, for a total of six measurements per sample).[3] The final F^- content was averaged from three independent solutions per sample.

Scanning electron microscopy (SEM) was performed with a Phenom ProX desktop electron microscope. The powdered samples were spread onto carbon tape and images were collected in backscattered electron mode (BSE) with an acceleration voltage of 10 keV.

The analysis of the Ni oxidation state was carried out by X-ray photoelectron spectroscopy (XPS) using a DAR 400 instrument (Omicron) with an Al-K_α line (1486 eV, 250 W) as the X-ray source and an EA 125X Hemispherical Energy Analyzer (Omicron). Survey scans were performed with a pass energy of 100 eV, and detailed scans of the Ni 3p region were performed with a pass energy of 30 eV. The spectra were fitted and analyzed using the CasaXPS software.

Results and discussion

In previous investigations on the n = 1 oxyfluorides $La_2NiO_3F_2$ and $La_2NiO_{2.5}F_3$, we demonstrated that isothermal *in situ* X-ray

powder diffraction can be used to obtain insight into the reaction intermediates occurring during the fluorination reaction as well as to obtain suitable parameters for bulk synthesis.[50] We also showed that the use of precursor oxides obtained from soft chemistry is beneficial for obtaining phase-pure oxyfluorides, most probably due to smaller particle sizes.[19,47] This is why we started our investigations with *in situ* XRD experiments for the fluorination of $La_4Ni_3O_{10}$ obtained from citrate synthesis.

Structural and compositional characterization of $La_4Ni_3O_{8.4}F_{3.5}$

Different oxide : PVDF ratios (1 : 1, 1 : 1.5, and 1 : 2) were initially tested and a single-phase product was obtained for the 1 : 2 ratio, corresponding to a nominal content of 4 F^- per f.u. The *in situ* XRD data obtained for the 1 : 2 reaction mixture at 370 °C is shown in Fig. 2 and the diffraction patterns of the precursor oxide (bottom) and the reaction product (top) are additionally given. From the additional reflections found in the time range of 4–7 h in the contour plot of Fig. 2, it is apparent that the reaction to the final oxyfluoride proceeds *via* one reaction intermediate. This intermediate possesses a larger unit cell than the oxide, which is indicated by the significant shift of (117) as well as (200)/(020) (please note that all (*hkl*) values are given with respect to the orthorhombic *Fmmm* coordinate system with *c* as the longest axis) to smaller *Q* values. Upon longer heating, the formation of the final oxyfluoride is achieved. Here, a clear shift of (200)/(020) to higher *Q* values indicates a decrease in the size of the basal *ab*-plane, which is accompanied by a further elongation of *c* as the most intense (117) signal shifts to even lower *Q* values. The observation of a distinct reaction intermediate is in contrast to the reaction of the closely related compound $La_4Co_3O_{10}$ with PVDF, where the product $La_4Co_3O_{10}F_2$ is formed directly.[38] For the *n* = 1 nickelates, on the other hand, the presence of several reaction intermediates was previously found.[50] Efforts to isolate the intermediate of the fluorination reaction through targeted synthesis as well as quenching remained unsuccessful. From quenching experiments, a range of samples was obtained, which appeared to be mixtures of the precursor oxide and the final fluorination product. To extract the unit cell parameters of the intermediate, Le Bail fits to the *in situ* XRD data were performed in the *Fmmm* space group. The following unit cell dimensions were obtained for the 370 °C data: *a* = 5.662 Å, *b* = 5.705 Å, and *c* = 29.223 Å. Full structure refinements were not attempted as the present data quality is not sufficient enough. Nonetheless, the detailed investigation of the formation reaction is planned for a future publication.

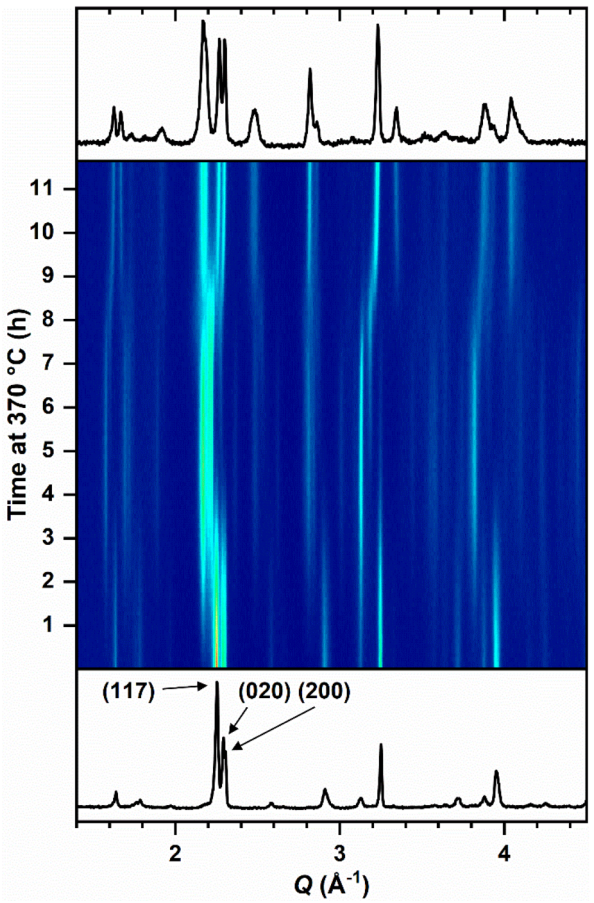

Fig. 2 Time dependent *in situ* XRD patterns of the reaction of $La_4Ni_3O_{10}$ with PVDF (molar ratio: 1 : 2) obtained at 370 °C. Bottom and top diffraction patterns are the initial and final patterns.

Bulk synthesis of the oxyfluoride was performed with oxide : PVDF mixtures (1 : 2 ratio) at 370 °C for 16 h. This results in the highly fluorinated black product $La_4Ni_3O_{8.4}F_{3.5}$. SEM investigations reveal irregularly shaped particles with diameters of 0.5–1 μm (see Fig. S2†). The morphology of these particles does not differ significantly from the particles of the starting oxide. IR spectra (see Fig. S3†) show high absorption in the entire range of 4000 to 400 cm^{-1}, with no signals of PVDF, indicating the absence of residual PVDF or other carbon related impurities in the resulting product. The fluoride content of the oxyfluoride was determined using a fluoride ion sensitive electrode by applying the standard addition technique. The obtained value of 7.15(4)% corresponds to 3.5(2) F^- per formula unit, which is clearly less than the nominal value of 4 F^- per f.u. expected from the amount of PVDF used. This deviation reveals that not all fluorine from the PVDF is incorporated into the oxide lattice. A similar finding was observed in the synthesis of $La_{0.5}Sr_{3.5}Fe_3O_{7.5}F_{2.6}$ where 3 F^- per f.u. are expected from the amount of PVDF used. Based on these findings, synthesis experiments with an extended range of oxide : PVDF ratios were performed in finer steps (see diffraction patterns in Fig. S4†). It was found that the 1 : 1.75 oxide : PVDF ratio (nominally 3.5 F^- per f.u.) also results in a phase-pure product but with slightly decreased lattice parameters. This points to a rather wide accessibility range of the oxyfluoride. The structural investigations of the here presented work (*vide infra*) were nevertheless performed for the 1 : 2 product; hence, neutron diffraction data were obtained for this compound. Assuming La^{3+} and taking into account the result of the XRF measurement (La/Ni = 1.31; which is in good agree-

ment with the nominal molar ratio of 1.33), in combination with the results of the iodometric titration, it can be concluded that Ni has an average oxidation state of 2.76(11) in the oxyfluoride, which is comparable to the obtained average oxidation state of Ni in the precursor oxide of 2.68(4). According to this value and with 3.5 fluoride ions per f.u., the oxyfluoride should contain ~8.4 O^{2-} per f.u. for charge neutrality. XPS spectra were obtained for the oxide and the oxyfluoride. This enables a comparison of the surface oxidation state of nickel in both samples. Due to a heavy overlap of the Ni $2p_{3/2}$ and the La $3d_{3/2}$ peaks,[19,46,51,52] the less well resolved Ni 3p peak was investigated. The corresponding spectra are given in Fig. S5 in the ESI.† The observed signal can be interpreted as an overlap of the Ni^{2+} signal at ~67.0 eV and the Ni^{3+} signal at 70.7 eV.[53] Upon fluorination, a decrease of the Ni^{2+} signal is observed, pointing to a decrease of Ni^{2+} species at the sample surface, which is in concordance with the slight increase of the Ni oxidation state as found by iodometric titration. In order to verify the oxygen content, thermogravimetric analysis in a reducing atmosphere (50 mL min^{-1} of 5% H_2 in N_2) was performed (see Fig. S6†). It was found that nickel is reduced to its metallic state under the applied conditions, which was verified by a field dependent magnetization measurement at 300 K showing ferromagnetic behavior (see Fig. S7†). On the other hand, in the XRD pattern of the reduction product (see Fig. S8†), only LaOF could be identified, implying that nickel is amorphous. This decomposition reaction was also investigated by *in situ* XRD (*vide infra*). Given these products and the observed weight loss of 7.45% during the reduction process, an initial oxygen stoichiometry of 8.4 is confirmed, which is in good agreement with the expected value. Therefore, the sum formula $La_4Ni_3O_{8.4}F_{3.5}$ can be deduced for the title compound. The presence of ~12 anions per formula unit demands for fully occupied interstitial anion positions, which is in agreement with the results from refinement of neutron powder diffraction data (*vide infra*).

Laboratory X-ray diffraction patterns of oxyfluoride samples from different batches are shown in Fig. 3. Based on these data, a significant anisotropic broadening of selected reflections (like (117)/(11−7)) is evident. This broadening is similar for all batches and is also found in the diffraction pattern presented by C. K. Blakely *et al.* for a compound denoted $La_4Ni_3O_8F_2$, which was obtained from fluorination of $La_4Ni_3O_8$ with XeF_2 as the fluorination agent.[39] The authors indexed their diffraction pattern with an orthorhombic unit cell even though the same splitting of (117)/(11−7) is clearly visible in their data. This anisotropic reflection broadening is most likely the result of stacking faults in the perovskite like layer, *i.e.* the random appearance of perovskite slabs with deviating layer thickness *n*. Such stacking faults are common for Ruddlesden–Popper compounds and result in the observed broadening of all (*hkl*) reflections with $l \neq 0$.[54–57] Clearly, the anisotropic broadening interferes with the structural determination from laboratory X-ray diffraction data alone, which is why we performed different post-synthetic annealing experiments aiming to reduce the peak broadening. For the *n* = 2

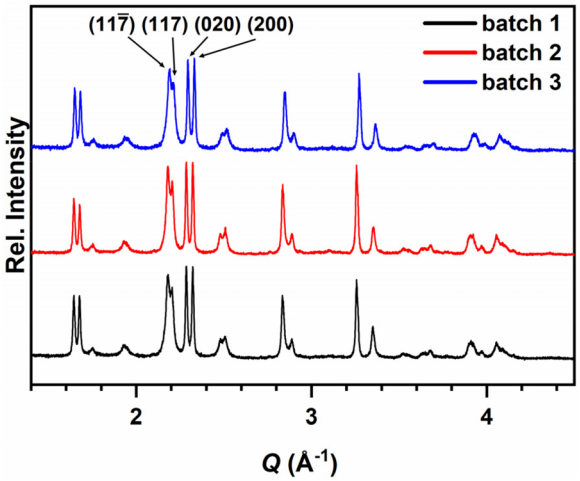

Fig. 3 XRD patterns of $La_4Ni_3O_{8.4}F_{3.5}$ from different batches. The indices are given for the (117)/(11−7) and (200)/(020) reflexes, indicating the difference in reflection broadening.

compound $La_3Ni_2O_{5.5}F_{3.5}$, an improvement in the crystallinity upon heating in evacuated silica ampules was reported but unfortunately no X-ray diffraction patterns of the crude or the annealed product were observed, which would allow for a comparison with the reflection broadening observed here.[35] We annealed our oxyfluoride samples in evacuated glass ampules for 5 days at 350 °C, but unfortunately none of the experiments resulted in significantly sharper peaks.

Structural refinement was performed as joint refinement combining laboratory XRD with neutron powder diffraction data. The above discussed splitting of (117)/(11−7) demands for a monoclinic unit cell symmetry and indexing of the XRD-data was possible in the space groups $P2_1/a$ (the space group of the starting oxide; please note the non-standard setting with *c* as the longest axis, enabling an easier comparison with the *I*4/*mmm* archetype) and $A2/a$ (the space group recently reported for the closely related oxyfluoride $La_4Co_3O_{10}F_2$).[38] In a subsequent Le Bail fit of the NPD data in $A2/a$, some reflections occurred, which should be integrally extinct in an *A*-centered lattice. These reflections can be indexed as (123), (027), and (207) (see Fig. S9†) and a primitive unit cell is thus derived for $La_4Ni_3O_{8.4}F_{3.5}$. The subsequent structural refinement was therefore performed in $P2_1/a$ with $Z = 4$ and $a = 5.4206(3)$ Å, $b = 5.5081(3)$ Å, $c = 29.9823(18)$ Å, and $\beta = 90.85(4)$. The anisotropic peak broadening was taken into account by applying the Stephens model for general strain broadening.[58] To limit the number of refinable parameters, the anisotropic strain parameters were constrained to be the same for both patterns (since the samples were from the same batch). Additionally, the thermal displacement parameters were constrained to be identical for the same type of atoms. The Rietveld plots obtained for the refinements in $P2_1/a$ are given in Fig. 4 and the refined crystallographic parameters are listed in Table 1. Fluorination results in the elongation of the *c* axis of about 2 Å compared to the starting oxide $La_4Ni_3O_{10}$: $P2_1/a$, $a = 5.4234$ Å,

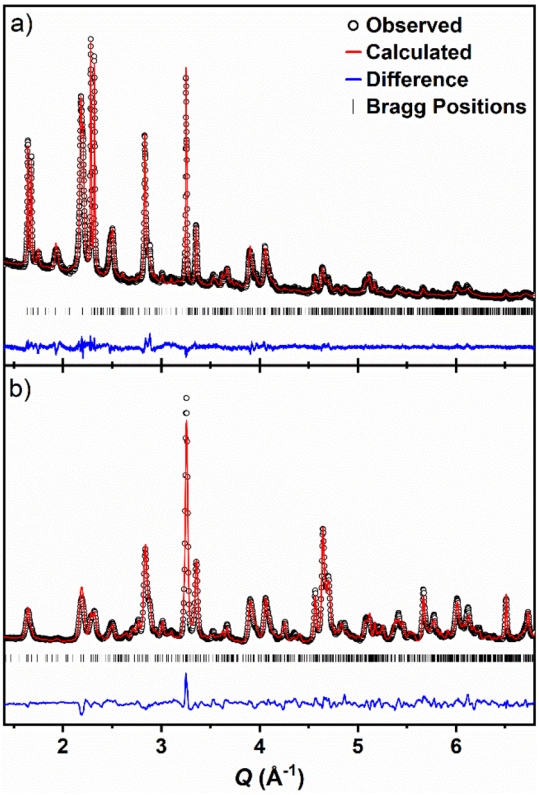

Fig. 4 Rietveld plots of the joint refinements against (a) X-ray (λ = 1.542 Å) and (b) neutron diffraction data (λ = 1.594 Å) in the space group $P2_1/a$.

b = 5.4732 Å, c = 28.0041 Å, and β = 90.15°,[59] which is indicative of the insertion of F^- into the interstitial sites of the rock salt layer, and indeed a full occupation of this interstitial position is found from refining the occupation of this position. Additionally, an increase of b and therefore of the distortion of the basal ab-plane is observed, which is accompanied by an increase in the monoclinic angle β. Both observations are the result of an increased tilting distortion of the $Ni(O,F)_6$ octahedra compared to the starting oxide. This is different from the structure of $La_4Co_3O_{10}F_2$, where the fluorination results in a stronger elongation of c (~3 Å) that is accompanied by a decrease of the ab-distortion, a β value close to 90° and smaller tilting components of the perovskite octahedra.[38] Such different structural behavior upon fluorination is in line with the results obtained for the n = 1 oxyfluorides of nickel and cobalt. Here, the Co-oxyfluoride shows a similar strong elongation of c (~2.6 Å) and a decrease of the ab-distortion.[27] For the Ni-oxyfluorides $La_2NiO_3F_2$ and $La_2NiO_{2.5}F_3$ on the other hand, less pronounced elongations in c are accompanied by strong changes in ab and a significant increase of the octahedra tilting even though no full interlayer occupation was found for the Ni-oxyfluorides.[19,46] In the refinements, the site occupation factors were fixed to unity after preliminary tests due to the limited quality of the present data. Attempts to refine the anionic occupation factors or the isotropic thermal displacement parameters resulted in unrealistic values due to highly correlated parameters and the strong anisotropic reflection broadening. The difference Fourier map obtained for the NPD data gave no hints for partial anion occupation. Therefore, SOF values were used for all anion positions, which is in concordance with the results of the chemical analysis. As the

Table 1 Structural parameters of $La_4Ni_3O_{8.4}F_{3.5}$ obtained from joint Rietveld refinements of XRD and ND data[a]

Atom	Anion site	x/a	y/b	z/c	U_{iso} [Å^2]	Occ.	Wyck.
La(1)		0.4945(2)	0.5037(13)	0.4343(19)	0.0160	1	4*e*
La(2)		0.0087(7)	0.4969(18)	0.0667(2)	0.0160	1	4*e*
La(3)		0.0786(2)	1.0019(16)	0.3117(3)	0.0160	1	4*e*
La(4)		0.5015(2)	1.0032(17)	0.1942(3)	0.0160	1	4*e*
Ni(1)		1/2	0	1/2	0.0073	1	2*b*
Ni(2)		0	0	0	0.0073	1	2*a*
Ni(3)		0.0050(3)	0.5030(3)	0.3705(3)	0.0073	1	4*e*
Ni(4)		0.0085(3)	0.9966(3)	0.1236(4)	0.0073	1	4*e*
O/F(1)	*te*	0.2568(10)	0.2419(6)	0.1422(17)	0.0167	1	4*e*
O/F(2)	*te*	0.2804(9)	0.7115(6)	0.3638(14)	0.0167	1	4*e*
O/F(3)	*te*	0.2524(7)	0.7426(5)	0.6227(15)	0.0167	1	4*e*
O/F(4)	*te*	0.2629(9)	0.7562(6)	0.1195(16)	0.0167	1	4*e*
O/F(5)	*ta*	−0.0022(8)	0.4765(7)	0.3146(11)	0.0167	1	4*e*
O/F(6)	*ta*	0.0278(8)	0.9468(7)	0.1930(12)	0.0167	1	4*e*
O/F(7)	*ca*	0.4892(9)	0.9489(8)	0.4345(13)	0.0167	1	4*e*
O/F(8)	*ca*	0.5026(7)	0.4400(7)	0.0611(13)	0.0167	1	4*e*
O/F(9)	*ce*	0.2121(9)	0.7835(7)	0.5025(11)	0.0167	1	4*e*
O/F(10)	*ce*	0.2525(7)	0.7521(7)	0.0102(12)	0.0167	1	4*e*
F(1)	*i*	0.2535(9)	0.2297(5)	0.2512(13)	0.0105	1	4*e*
F(2)	*i*	0.2143(11)	0.7253(5)	0.2595(12)	0.0105	1	4*e*

Space group: $P2_1/a$ (14)
a = 5.4206(3) Å, b = 5.5081(3) Å, c = 29.9823(18) Å
$\alpha = \gamma$ = 90°, β = 90.85(4)°
V = 895.10(6) Å^3
R_w = 5.44%, χ^2 = 1.33, GOF = 1.15

[a] Octahedral anion sites have a 85%/15% oxide/fluoride occupation. The sum formula is taken as $La_4Ni_3O_{8.5}F_{3.5}$.

almost identical scattering lengths of O and F do not allow a clear assignment of the remaining 1.5 F^- to specific positions, we performed additional bond valence sum analysis (BVS) for selected anion distributions (results are shown in Table S1†). All models in which the terminal apical O/F(6) site is solely occupied by F^- gave a significantly reduced global instability index (GII) of ~8% compared to statistical distribution (GII: ~11%). The tested model with the lowest global instability index (GII: 7.7%) involves full occupation of the O/F(6) site by F^- and occupation of one quarter of each of the central equatorial anion sites (O/F(9) and O/F(10)). This distribution is unusual, as occupation of the equatorial sites has never been observed in other RP oxyfluorides. Another model takes the short atomic distance of Ni(4)–O/F(5) into account and comes with a full occupation of the O/F(6) site by F^-, full occupation of O/F(5) by O^{2-} and a statistical distribution of the remaining F^- over the other octahedral anion sites. The GII of this model (7.9%) is nearly as low as the one mentioned above. It is therefore very likely for the O/F(6) site to be occupied only by F^-, whereas a clear statement about the distribution of the remaining 0.5 F^-/f.u. is not unambiguously possible. We therefore opted for a statistical distribution of the remaining F^- to the remaining anion positions (please note that the atoms of these positions are shown as oxygen in Fig. 5). To obtain charge neutrality, nickel has to be partially in the +2 oxidation state. The Ni(4) site has the lowest BVS; we therefore choose an 0.5 : 0.5 occupation of this site by Ni^{3+} and Ni^{2+}.

The structure derived from the Rietveld refinements is shown in Fig. 5 and the atomic distances and angles are reported in the ESI (Tables S2 and S3†). A strong tilting of the octahedra is apparent and additionally all four different octahedra are clearly distorted. This is especially true for the terminal octahedra, which include three different anion positions. The terminal apical anion position deviates in a way that this position seems to not follow the overall tilt of the octahedra (compare Fig. 5 and S10†). Interestingly, similarly strong distorted octahedra were reported for $La_4Ni_3O_{10}$, and $La_4CoO_{10}F_2$, especially showing the deflection of the terminal apical anion position.[38,59] On the other hand, the anion positions are subject to an increased uncertainty due to the strong reflection broadening in combination with the complexity of the structure and the resulting high number of refinable variables. For a more precise structural description, diffraction data with less anisotropic broadening would be needed. Alternatively, modeling of the stacking faults with the FAUTLS/DIFFaX[60,61] program might enable a better refinement of the diffraction data.

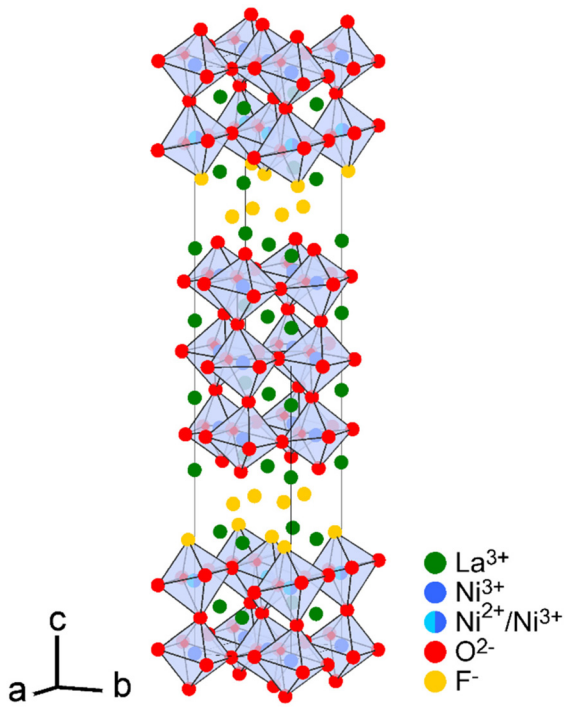

Fig. 5 Crystal structure of $La_4Ni_3O_{8.4}F_{3.5}$ (space group: $P2_1/a$) with representation of Ni-coordination polyhedra.

Thermal stability

To investigate the thermal stability of the oxyfluoride, temperature dependent XRD measurements up to 900 °C were performed on a laboratory diffractometer in dynamic gas atmospheres (40 mL min^{-1}) of N_2, air, and O_2 using a homemade '*Norby like*' capillary reactor,[62] which was modified in order to position the transfer capillary of a mass spectrometer close to the sample surface (see Fig. S1† for a sketch and a photograph). With this setup, we were able to analyze the evolved gases, gaining a deeper knowledge of such reactions. The thermal evolution of the diffraction patterns in the region of the most intense peaks are shown as contour plots in Fig. 6. The decomposition proceeds *via* two reaction intermediates, which are clearly visible from the appearance of additional peaks in the temperature region of 500 to 620 °C in all 3 contour plots. From the *in situ* MS data obtained in a N_2 atmosphere (compare Fig. S11†), a release of oxygen was found to be linked with the formation of the decomposition intermediates. The oxygen release was also observed in additional thermogravimetric experiments, indicating that ~0.5 O per formula unit is released in the first step (as shown in the ESI Fig. S12†). The formation of the first decomposition intermediate is therefore linked to a partial reduction of Ni^{3+} to Ni^{2+}, while the full reduction of all Ni^{3+} atoms to Ni^{2+} would result in the release of ~1.25 O per formula unit, which is found when combining the mass loss of both intermediates. The decompositon reaction is clearly linked to the oxygen partial pressure of the reaction atmosphere, which leads to different onset temperatures (defined as the temperature step where the first signals of the next phase are observable) depending on the reaction atmosphere. During heating in N_2, an onset temperature of 490 °C is observed, which increases to 510 °C in air and 530 °C in O_2. It is noteworthy that the decomposition intermediates observed here are not the same as the formation intermediate found in the fluorination reaction (see Fig. 2). The first decomposition intermediate has a smaller unit cell than $La_4Ni_3O_{8.4}F_{3.5}$, reflected by the signifi-

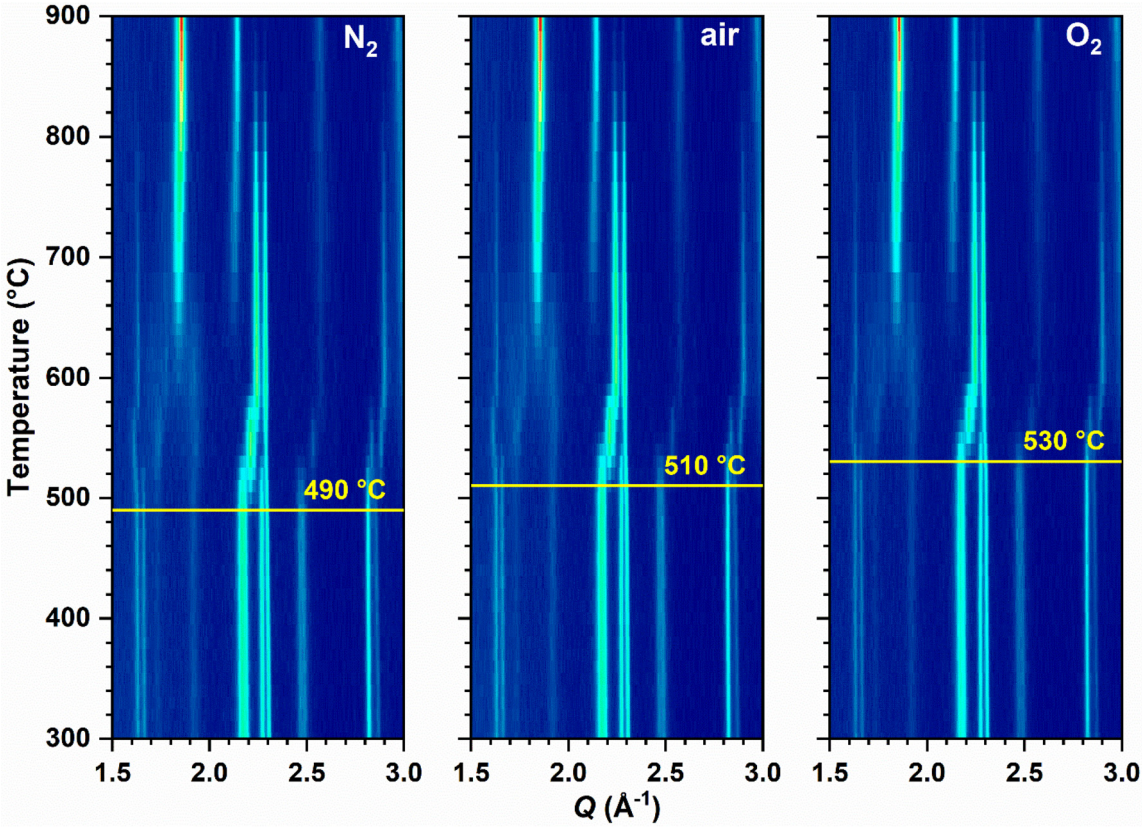

Fig. 6 Contour plots of the *in situ* XRD patterns obtained for the thermal decomposition of $La_4Ni_3O_{8.4}F_{3.5}$ in different atmospheres. The start of the decomposition is highlighted by a yellow line in each plot.

cant shift in the main reflections towards higher Q values. With increasing temperature, the sample further releases oxygen (see the TG-MS results in Fig. S12†) and the reflections of an n = 3 RP-phase similar to the starting oxide are observed as second decomposition intermediate. In all cases, LaOF and NiO were identified as final decomposition products above 650 °C as is often observed upon decomposition of La containing RP oxyfluorides.[19,46] When performing the *in situ* XRD-MS experiment in a reducing atmosphere (10% H_2 in N_2, compare Fig. S13†) LaOF is observed as the decomposition product, while signals of Ni(0) are not found. This is most probably the result of a weak amorphous contribution to the diffraction pattern, which is in contrast to the hard character of the Mo radiation used (please note that even the amorphous contribution of the glass capillary is missing from the diffraction data). From this experiment, it is additionally found that the reductive decomposition of $La_4Ni_3O_{8.4}F_{3.5}$ proceeds *via* at least two intermediates, which were not further investigated yet but clearly differ from the above observed decomposition intermediates. Such partially reduced oxyfluorides are of high interest and attempts to isolate them will be pursued in future studies. The thermal stability of the title compound is comparable to the n = 1 nickel-based oxyfluoride $La_2NiO_3F_2$ (~450 °C), while the higher fluorinated compound $La_2NiO_{2.5}F_3$ exhibits a significantly lower thermal decomposition temperature (~380 °C).[19,46,47]

Magnetic properties

The precursor oxide $La_4Ni_3O_{10}$ has previously been reported to be a Pauli paramagnet as a result of electron exchange between nickel sites with two different oxidation states (Ni^{2+} and Ni^{3+}). A weak susceptibility minimum around 90 K is additionally linked to a metal-to-metal transition.[63,64] This magnetic behaviour was also found for the precursor oxide of this study for which the χ_{mol} *vs.* T data are shown in Fig. 7a. Upon fluorination, a strong impact on the exchange interactions between different perovskite slabs is expected and was previously observed for $La_4Co_3O_{10}F_2$[38] and nickelate oxyfluorides with n = 2 and n = 1.[35,46,47] The results of the temperature dependent susceptibility measurements for $La_4Ni_3O_{8.4}F_{3.5}$ in an external field of 5 T are shown in Fig. 7(b) and reflect a Curie–Weiss behavior. As the inverse susceptibility shows a clear curvature, the data were fitted with an extended Curie–Weiss law $\frac{1}{\chi_{mol}} = \frac{1}{\frac{C}{T-\theta} + \chi_0}$ compromising a temperature independent contribution (χ_0). The fit is shown in Fig. 7b and the obtained Curie constant of 5.31 cm^3 K mol^{-1} corresponds to a paramagnetic moment of μ_{eff} = 1.06μ_B per Ni atom. This is lower than the value of 2.04μ_B expected for Ni with an observed average oxidation state of 2.76 and Ni^{3+} being in a low-spin configuration. If Ni^{3+} is considered to be in a high-spin con-

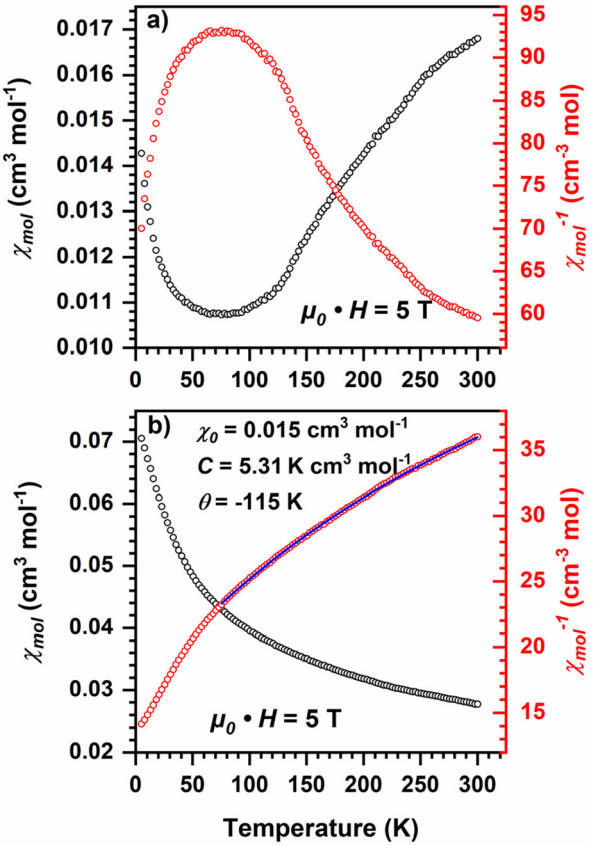

Fig. 7 Temperature dependent susceptibility (black) and inverse susceptibility (red) data of (a) $La_4Ni_3O_{10}$ and (b) $La_4Ni_3O_{8.4}F_{3.5}$ at 5 T. For the oxyfluoride, the inverse susceptibility was fitted using an extended Curie–Weiss law (blue line) in the range of 75 K to 300 K.

figuration, the expected moment would be 3.65μ_B, which is even larger than the observed value. However, it should be kept in mind that the Curie–Weiss law in principle only applies to isolated ions, which is why such values should not be overinterpreted. Furthermore, the value of C, and in turn of μ_{eff}, is highly dependent on the temperature interval used for the fit. The Weiss temperature of $\theta \approx -115$ K is indicative of antiferromagnetic interactions but no clear sign of a long-range magnetic ordering was observed, neither in the 5 T nor in the 0.1 T data (see Fig. S14†). Our investigations show that fluorination strongly alters the magnetic properties compared to the parent oxide most probably due the partially oxidation of Ni^{2+} to Ni^{3+}, resulting in less delocalized electrons.

Conclusions

The Ruddlesden–Popper oxyfluoride $La_4Ni_3O_{8.4}F_{3.5}$ with a mixed $Ni^{2+/3+}$ oxidation state was prepared for the first time by topochemical fluorination of a $La_4Ni_3O_{10}$ precursor from the citrate synthesis with PVDF as the fluorine source. The chemical composition of this compound was confirmed by several analytical methods. $La_4Ni_3O_{8.4}F_{3.5}$ crystallizes in the same space group as the parent oxide ($P2_1/a$), and the presence of strongly anisotropic broadened (hkl) reflections with $l \neq 0$ points to stacking faults related to the thickness of the perovskite layers. The title compound is stable up to 510 °C in air (490 °C in N_2 and 530 °C in O_2) and the thermal decomposition is accompanied by the release of oxygen as found by XRD-MS and TG-MS measurements. $La_4Ni_3O_{8.4}F_{3.5}$ is a Curie–Weiss magnet with a Weiss constant of $\theta \approx -115$ K, indicating antiferromagnetic interactions. The observed paramagnetic magnetic moment of μ_{eff} = 1.84μ_B points to a low-spin configuration of Ni^{3+}.

Author contributions

J. G.: conceptualization, formal analysis, investigation, methodology, visualization, and writing – original draft. S. G. E.: supervision, resources, and writing – review & editing. J. J.: supervision, conceptualization, data curation, investigation, formal analysis, visualization, and writing – review & editing.

Conflicts of interest

The authors declare that they have no known competing financial interests or personal relationships that could have appeared to influence the work reported in this paper.

Data availability

The data supporting the findings of this study are available within the article and its ESI.† The crystallographic data of $La_4Ni_3O_{8.4}F_{3.5}$ have been deposited at the CCDC under deposition number 2451197,† and can be obtained from **https://www.ccdc.cam.ac.uk/**. The neutron diffraction data are available under the following link **https://doi.ill.fr/10.5291/ILL-DATA.5-23-769**. Any other information should be requested from the corresponding authors.

Acknowledgements

The neutron diffraction experiment was performed on the D2B diffractometer run by the Institut Laue-Langevin (ILL); beamtime was granted under the proposal number 5-23-769.[48] We thank Dr. Clemens Ritter for performing the measurement, and we thank the ILL for the allocated beamtime. We thank Eik Koslowski for performing the XPS measurements.

References

1 S. Liu, M. Avdeev, Y. Liu, M. R. Johnson and C. D. Ling, *Inorg. Chem.*, 2016, **55**, 1403–1411.
2 Z. Li, W. Guo, T. T. Zhang, J. H. Song, T. Y. Gao, Z. B. Gu and Y. F. Nie, *APL Mater.*, 2020, **8**, 091112.

3 A. Bivour, J. Jacobs, F. Daumann, G. Hörner, B. Weber, C. Ritter and S. G. Ebbinghaus, *Inorg. Chem.*, 2024, **63**, 20427–20437.
4 X. Sun, Y. Mi, F. Jiao and X. Xu, *ACS Catal.*, 2018, **8**, 3209–3221.
5 G. Gou, M. Zhao, J. Shi, J. K. Harada and J. M. Rondinelli, *Chem. Mater.*, 2020, **32**, 2815–2823.
6 T. Nagai, H. Shirakuni, A. Nakano, H. Sawa, H. Moriwake, I. Terasaki and H. Taniguchi, *Chem. Mater.*, 2019, **31**, 6257–6261.
7 K.-E. Hasin, N. Pokhrel and E. A. Nowadnick, *Chem. Mater.*, 2024, **36**, 7552–7560.
8 H. Yaguchi, K. Fujii, Y. Tsuchiya, H. Ogino, Y. Tsujimoto and M. Yashima, *ACS Appl. Energy Mater.*, 2022, **5**, 295–304.
9 N. A. Tarasova, *Chim. Techno Acta*, 2022, **9**, 20229415.
10 J. W. González, A. M. León, C. González-Fuentes and R. A. Gallardo, *Nanoscale*, 2025, **17**, 4796–4807.
11 F. Bernardini, M. Fiebig and A. Cano, *J. Appl. Phys.*, 2025, **137**, 103903.
12 C. Park and R. L. Snyder, *Appl. Supercond.*, 1995, **3**, 73–83.
13 H. Sun, M. Huo, X. Hu, J. Li, Z. Liu, Y. Han, L. Tang, Z. Mao, P. Yang, B. Wang, J. Cheng, D.-X. Yao, G.-M. Zhang and M. Wang, *Nature*, 2023, **621**, 493–498.
14 O. J. Hernandez, G. Geneste, T. Yajima, Y. Kobayashi, M. Okura, K. Aidzu, C. Tassel, S. Paofai, D. Swain, C. Ritter and H. Kageyama, *Inorg. Chem.*, 2018, **57**, 11058–11067.
15 H. Sonoki, D. Mori, S. Taminato, Y. Takeda, O. Yamamoto and N. Imanishi, *Chem. Commun.*, 2019, **55**, 7454–7457.
16 Y. Bréard, B. Raveau, D. Pelloquin and A. Maignan, *J. Mater. Chem.*, 2007, **17**, 2818–2823.
17 D. Pelloquin, N. Barrier, D. Flahaut, V. Caignaert and A. Maignan, *Chem. Mater.*, 2005, **17**, 773–780.
18 O. Clemens and P. R. Slater, *Rev. Inorg. Chem.*, 2013, **33**, 105–117.
19 J. Jacobs, M. A. L. Marques, H.-C. Wang, E. Dieterich and S. G. Ebbinghaus, *Inorg. Chem.*, 2021, **60**, 13646–13657.
20 C. S. Knee and M. T. Weller, *Chem. Commun.*, 2002, 256–257.
21 A. L. Hector, J. A. Hutchings, R. L. Needs, M. F. Thomas and M. T. Weller, *J. Mater. Chem.*, 2001, **11**, 527–532.
22 Y. Bréard, C. Michel, M. Hervieu and B. Raveau, *J. Mater. Chem.*, 2000, **10**, 1043–1045.
23 E. E. McCabe and C. Greaves, *J. Fluor. Chem.*, 2007, **128**, 448–458.
24 F. Galasso and W. Darby, *J. Phys. Chem.*, 1962, **66**, 1318–1320.
25 L.-S. Du, F. Wang and C. P. Grey, *J. Solid State Chem.*, 1998, **140**, 285–294.
26 G. S. Case, A. L. Hector, W. Levason, R. L. Needs, M. F. Thomas and M. T. Weller, *J. Mater. Chem.*, 1999, **9**, 2821–2827.
27 M. A. Nowroozi, S. Ivlev, J. Rohrer and O. Clemens, *J. Mater. Chem. A*, 2018, **6**, 4658–4669.
28 L. D. Aikens, L. J. Gillie, R. Li and C. Greaves, *J. Mater. Chem.*, 2002, **12**, 264–267.
29 T. Baikie, E. L. Dixon, J. F. Rooms, N. A. Young and M. G. Francesconi, *Chem. Commun.*, 2003, 1580–1581.
30 P. R. Slater and R. K. B. Gover, *J. Mater. Chem.*, 2002, **12**, 291–294.
31 T. Sivakumar and J. B. Wiley, *Mater. Res. Bull.*, 2009, **44**, 74–77.
32 R. Zhang, G. Read, F. Lang, T. Lancaster, S. J. Blundell and M. A. Hayward, *Inorg. Chem.*, 2016, **55**, 3169–3174.
33 Y. Tsujimoto, K. Yamaura, N. Hayashi, K. Kodama, N. Igawa, Y. Matsushita, Y. Katsuya, Y. Shirako, M. Akaogi and E. Takayama-Muromachi, *Chem. Mater.*, 2011, **23**, 3652–3658.
34 R. L. Needs and M. T. Weller, *J. Chem. Soc., Dalton Trans.*, 1995, 3015–3017.
35 R. Zhang, M. S. Senn and M. A. Hayward, *Chem. Mater.*, 2016, **28**, 8399–8406.
36 K. Wissel, T. Vogel, S. Dasgupta, A. D. Fortes, P. R. Slater and O. Clemens, *Inorg. Chem.*, 2020, **59**, 1153–1163.
37 N. N. M. Gurusinghe, J. C. Fones, J. F. Marco, F. J. Berry and C. Greaves, *Dalton Trans.*, 2014, **43**, 2038–2043.
38 B. Gonano, Ø. S. Fjellvåg, G. Steciuk, K. Marshall, H. Fjellvåg and M. Valldor, *Scr. Mater.*, 2025, **255**, 116379.
39 C. K. Blakely, S. R. Bruno, S. K. Kraemer, A. M. Abakumov and V. V. Poltavets, *J. Solid State Chem.*, 2020, **289**, 121490.
40 P. R. Slater, *J. Fluor. Chem.*, 2002, **117**, 43–45.
41 P. R. Slater, P. P. Edwards, C. Greaves, I. Gameson, M. G. Francesconi, J. P. Hodges, M. Al-Mamouri and M. Slaski, *Phys. C*, 1995, **241**, 151–157.
42 C. Greaves, J. L. Kissick, M. G. Francesconi, L. D. Aikens and L. J. Gillie, *J. Mater. Chem.*, 1999, **9**, 111–116.
43 P. R. Slater, J. P. Hodges, M. G. Francesconi, C. Greaves and M. Slaski, *J. Mater. Chem.*, 1997, **7**, 2077–2083.
44 G. B. Peacock, I. Gameson, M. Slaski, J. J. Capponi and P. P. Edwards, *Phys. C*, 1997, **289**, 153–160.
45 M. Al-Mamouri, P. P. Edwards, C. Greaves, P. R. Slater and M. Slaski, *J. Mater. Chem.*, 1995, **5**, 913.
46 K. Wissel, J. Heldt, P. B. Groszewicz, S. Dasgupta, H. Breitzke, M. Donzelli, A. I. Waidha, A. D. Fortes, J. Rohrer, P. R. Slater, G. Buntkowsky and O. Clemens, *Inorg. Chem.*, 2018, **57**, 6549–6560.
47 J. Jacobs, H.-C. Wang, M. A. L. Marques, K. Xu, J. Schmedt Auf Der Günne and S. G. Ebbinghaus, *Inorg. Chem.*, 2024, **63**, 6075–6081.
48 S. G. Ebbinghaus, A. Bivour, J. Jacobs and C. Ritter, DOI: **10.5291/ILL-DATA.5-23-769**.
49 B. H. Toby and R. B. Von Dreele, *J. Appl. Crystallogr.*, 2013, **46**, 544–549.
50 J. Jacobs, A. Bivour, V. Sikolenko, H. Kohlmann, T. C. Hansen, J. R. Hester, K. Xu, J. Schmedt Auf Der Günne and S. G. Ebbinghaus, *J. Am. Chem. Soc.*, 2025, **147**, 9739–9751.
51 R. Clauberg, W. Gudat, E. Kisker, E. Kuhlmann and G. M. Rothberg, *Phys. Rev. Lett.*, 1981, **47**, 1314–1317.
52 J. F. Moulder, W. F. Stickle, P. E. Sobol and K. D. Bomben, *Handbook of X-ray Photoelectron Spectroscopy: A Reference Book of Standard Spectra for Identification and Interpretation*

of XPS Data, ed. J. Chastain, Perkin-Elmer Corporation, Physical Electronics Division, Eden Prairie, MN, 1992.
53 X. Ning, Z. Wang and Z. Zhang, *Sci. Rep.*, 2015, **5**, 8460.
54 A. Jarvis, F. J. Berry, J. F. Marco, M. Sanchez-Arenillas, G. Cibin, O. Clemens and P. R. Slater, *J. Solid State Chem.*, 2020, **287**, 121372.
55 R. Seshadri, M. Hervieu, C. Martin, A. Maignan, B. Domenges, B. Raveau and A. N. Fitch, *Chem. Mater.*, 1997, **9**, 1778–1787.
56 M. Periyasamy, L. Patra, Ø. S. Fjellvåg, P. Ravindran, M. H. Sørby, S. Kumar, A. O. Sjåstad and H. Fjellvåg, *ACS Appl. Electron. Mater.*, 2021, **3**, 2671–2684.
57 A. S. Gorkusha, S. V. Cherepanova and S. V. Tsybulya, *J. Appl. Crystallogr.*, 2024, **57**, 1578–1587.
58 P. W. Stephens, *J. Appl. Crystallogr.*, 1999, **32**, 281–289.
59 S. Kumar, Ø. Fjellvåg, A. O. Sjåstad and H. Fjellvåg, *J. Magn. Magn. Mater.*, 2020, **496**, 165915.
60 M. Casas-Cabanas, J. Rodríguez-Carvajal, J. Canales-Vázquez, Y. Laligant, P. Lacorre and M. R. Palacín, *J. Power Sources*, 2007, **174**, 414–420.
61 M. M. J. Treacy, J. M. Newsam and M. W. Deem, *Proc. R. Soc. London, Ser. A*, 1991, **433**, 499–520.
62 P. Norby, *J. Am. Chem. Soc.*, 1997, **119**, 5215–5221.
63 M. U. Nagell, S. Kumar, M. H. Sørby, H. Fjellvåg and A. O. Sjåstad, *Phase Transitions*, 2015, **88**, 979–990.
64 M. D. Carvalho, M. M. Cruz, A. Wattiaux, J. M. Bassat, F. M. A. Costa and M. Godinho, *J. Appl. Phys.*, 2000, **88**, 544–549.